BIBECHANA
Vol. 23, No. 3, August 2026, 1–8

ISSN 2091-0762 (Print), 2382-5340 (Online)
Journal homepage: http://nepjol.info/index.php/BIBECHANA
Publisher:Dept. of Phys., Mahendra Morang A. M. Campus (Tribhuvan University)Biratnagar

Physical properties of hole-doped rutile TiO_2 using virtual crystal approximation

Kamal Khanal, Navin Sharma, Dipendra Prasad Kalauni, Mohan Bahadur Kshetri, Madhav Prasad Ghimire, Tika Ram Lamichhane*

Central Department of Physics, Tribhuvan University, Kirtipur, Kathmandu, Nepal.

*Corresponding author: Email: tika.lamichhane@cdp.tu.edu.np

Abstract

Titania (TiO_2) is a structurally stable multi-functional material having the semiconducting features suitable for optoelectronic applications. By using virtual crystal approximation (VCA) in DFT (GGA + mBJ) method, the pristine rutile TiO_2 has the direct band gap of 2.35 eV with non-magnetic semiconducting nature. It is active in visible as well as near-UV ranges. Furthermore, this pristine structure has the static refractive indices 2.16 (xx) and 2.37 (zz), while the dielectric constants 4.6 (xx) and 5.6 (zz-direction). Above 5.3 eV, the dielectric function is observed to have the negative real part, indicating plasmonic behavior. When considering hole-doping in rutile TiO_2 to the Ti-site, the dielectric constant has higher value. When doping concentration increases from 10% to 20%, the optical band gap changes from 3.10 eV to 3.61 eV. This shift is mainly due to interband transitions between O(2p) and Ti(3d) states. The obtained results show that the hole-doped rutile TiO_2 supports the optoelectronic applications.

Keywords
TiO_2, density functional theory, virtual crystal approximation, hole doping.

Article information
Manuscript received: April 3, 2026; Revised: May 22, 2026; Accepted: June 17, 2026
DOI: https://doi.org/10.3126/bibechana.v23i3.92526

1 Introduction

In 1972, Fujishima and Honda explained photoelectrochemical ability of titanium dioxide (TiO_2) which splits water into hydrogen and oxygen under ultraviolet radiation [1]. Since then, TiO_2 has remained at the forefront of materials research, with applications spanning photocatalysis, photovoltaics, dye-sensitized solar cells, gas sensing, electrochromic devices, batteries, coatings, ceramics, pigments, biomedical implants, corrosion protection, and even advanced electronic and spintronic technologies [2, 3]. Structurally, TiO_2 crystallizes in two major polymorphs–rutile and anatase-where metastable anatase converts to thermodynamically stable rutile phase at the elevated temperatures [4].

TiO_2 exhibits many desirable features such as low toxicity, durable stability, cost-effectiveness, resistant to corrosion, and strong redox potential [5, 6],

however; its photocatalytic performance is still obstructed by inherent drawbacks. In particular, the considerable band gap of TiO_2 (3.2 eV) limits its absorption to UV region, which represents small amount (nearly 4%) of solar radiation [6–8]. Due to this, TiO_2-based photocatalysts still suffer from poor use of solar energy because of their wide band gap and weak response to visible light. Many researchers have introduced different dopants into the TiO_2 lattice to address this limitation. These dopants modify the electronic structure, slows down recombination of electrons and holes, which improves its photocatalytic performance under solar irradiation [9, 10].

Investigations into TiO_2 doped with nitrogen and metallic dopants (Fe, Ag, and Ni) reported a reduced band gap over the range 2.0—2.4 eV, with $N/Ni/TiO_2$ sample exhibiting highest photocatalytic activity [11]. Stengl et al. [12] examined rare-earth ion doping (La, Ce, Pr, Nd, Sm, Eu, Dy, Gd) on TiO_2. They observed photo–activity toward visible light, which was due to reduction in band gap and better charge–carrier separation. Nd^{3+}–doped TiO_2 exhibited the best performance among the studied compositions. Similarly, Khlyustova et al. [13] observed doping TiO_2 with Al, Cu, Mo, and W led to lattice distortion and band gap reduction. As a result, photo–activity increased with Mo– and W–doped TiO_2 achieving up to 96% degradation efficiency under visible–light irradiation. Basera et al. [14] performed a DFT study on non-metal dopants (N, C, S and Se) in anatase TiO_2. Their results showed that Se interstitials are favorable p–type region, while N substitution is dominant in n–type region. Both doping configurations enhanced visible–light absorption and provided useful guidance for designing efficient photocatalysts. Similarly, a DFT study by Zahan et al. [15] demonstrated that Nb doping can transform rutile TiO_2 from a non–metallic state to a metallic or semi–metallic state, depending on dopant concentration. This transformation enhances electrical conductivity and extends optical absorption into the visible region, indicating improved photocatalytic potential. Zhou et al. [16] reported through DFT (LDA+U) that tensile strain in Al–doped anatase TiO_2 can transform deep localized acceptor levels into shallow delocalized ones, thereby enhancing hole mobility and enabling efficient p–type conductivity for improved photocatalytic performance. Several studies have examined doped TiO_2 using DFT and experimental methods, but the role of hole doping has not yet been clearly explained. This study aims to fill this gap, providing insights for design of efficient hole and spintronic multifunctional TiO_2–based materials.

2 Crystal structure and computational details

We explore the rutile phase of TiO_2, which crystallizes in a tetragonal structure belonging to the $P4_2/mnm$ (No. 136) space group. The initial geometry was constructed using experimentally determined lattice parameters measured at 15 K ($a = b = 4.586$ Å, $c = 2.954$ Å, $\alpha = \beta = \gamma = 90°$) [17]. The Wyckoff atomic positions used in the calculations are summarized in Table 1. The crystal structure and the first Brillouin zone corresponding to the tetragonal lattice are shown in Figure 1, where the key high-symmetry points are indicated. These provide the structural and reciprocal-space frameworks for the subsequent electronic and optical property analysis.

Table 1: Wyckoff position in rutile TiO_2

Atom	x	y	z
Ti	0	0	0
O	0.30469	0.30469	0

The physical properties of rutile TiO_2 were studied using DFT as using in FPLO code (version 22.00-64) [18]. All calculations were performed within the scalar-relativistic framework. To overcome band gap underestimation of standard DFT, two exchange–correlation schemes were employed: Perdew–Burke–Ernzerhof (PBE) generalized gradient approximation (GGA) [19] and modified Becke–Johnson (mBJ) potential [20, 21], which provides improved accuracy in predicting band gaps of semiconductors and insulators. To understand the effect of hole-doping on the system, we consider virtual crystal approximation (VCA) as performed in FPLO framework [18]. The Brillouin zone was sampled with $18 \times 18 \times 18$ Monkhorst–Pack k-point mesh for electronic structure calculations, while a $32 \times 32 \times 32$ grid was adopted for the computation of optical properties. The 10% and 20% Sc doping concentrations increases the modification of the electronic and optical properties by introducing hole carriers, altering the band structure, and enhancing the optical response of the TiO_2 .The self-consistent field (SCF) cycles were converged to within 1×10^{-8} Hartree for total energy and 1×10^{-6} Hartree/Bohr^3 for charge density. The dielectric function, $\varepsilon(\omega)$, was obtained using the `FOPTICS` module integrated within FPLO.

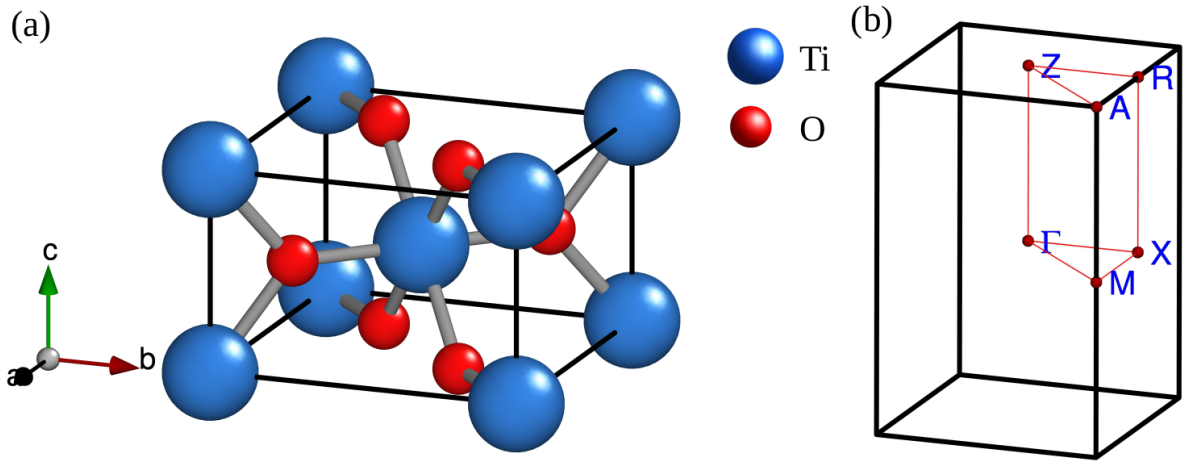

Figure 1: (a) Crystal structure of rutile TiO_2. (b) Corresponding first Brillouin zone with high-symmetry points

3 Results and discussion

3.1 Electronic properties

The calculated band gap of rutile TiO_2 using the GGA is 1.76 eV, which is lower than the experimental value (3.0 eV). There is a significant increase in band gap to 2.35 eV by employing the modified Becke–Johnson (mBJ) potential. This type of difference in experimental and calculated values may arise from the limitations of semilocal approximations and the absence of many-body effects in the present calculations.

Figure 2(a)–(c) represents band structure of rutile TiO_2 over −6 to 8 eV energy range, calculated using the GGA+mBJ approximation. In the pristine system, both VBM (valence band maximum) and CBM (conduction band minimum) are located at Γ point, confirming a direct band gap, as also reported in previous DFT studies [22,23]. The calculated valence-band width spans nearly 5.6 eV, quite similar to experimental value of 5.4 eV [24]. With 10% and 20% hole doping, the valence bands shift upward toward the Fermi level (E_f), with gap 2.58 eV and 2.88 eV respectively, indicating that hole doping systematically modifies the electronic structure and enhances p–type behavior of rutile TiO_2.

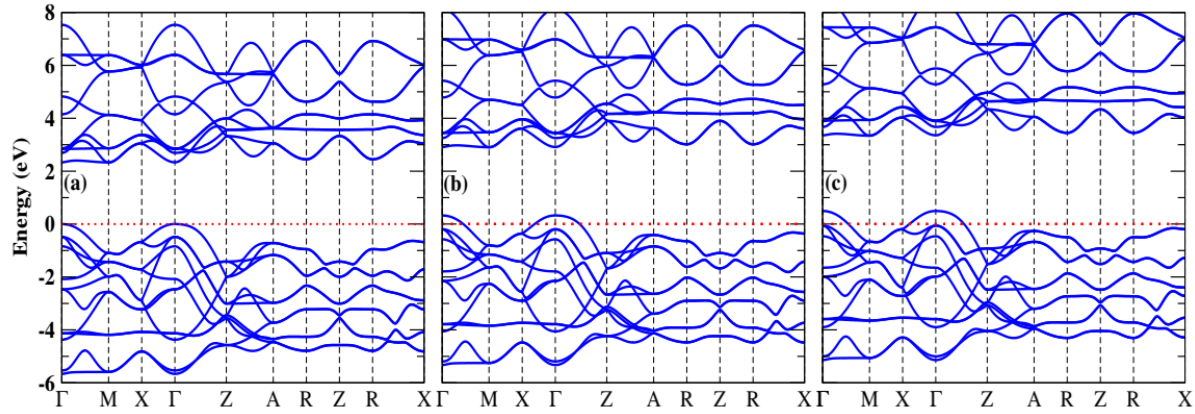

Figure 2: Band structures of rutile TiO_2: (a) pristine system, (b) 10% hole doping, and (c) 20% hole doping. Fermi level is shown by the red dotted line.

Figure 3(a)–(c) shows total and partial density of states of TiO_2. In pristine system, valence band region (−6 to 0 eV) comprises of O(2p) states, while conduction band (above nearly 2.5 eV) is dominated by Ti(3d) orbitals. This distribution gives well-known hybridization between O(2p) and Ti(3d) states and supports covalent bonding characteristics reported in earlier studies [25]. However, Ti(4p) states contribute only weakly. With 10% and 20% holes are doped, E_f shifts deeper into

O(2p) valence band, yielding to a higher DOS at E_f and confirming that holes occupy oxygen–derived states. Overall, these findings highlight a systematic transition of rutile TiO_2 from semiconducting behavior to quasi–metallic as the hole concentration increases.

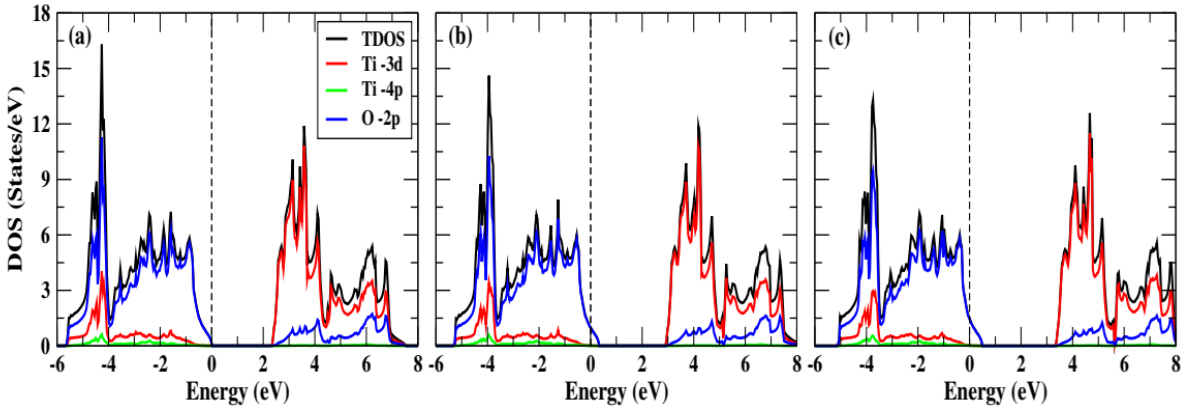

Figure 3: Total and partial DOS of rutile TiO_2: (a) pristine system, (b) 10% hole doping, and (c) 20% hole doping.

3.2 Optical properties

Basically, the important optical parameters are dielectric function ($\varepsilon(\omega) = \varepsilon_1(\omega) + i\varepsilon_2(\omega)$), loss function ($L$), optical conductivity (σ), refractive index (n), extinction coefficient (k), absorption coefficient (α), and reflectivity (R), each of which is frequency dependent [26–30]. These parameters related to rutile TiO_2 for both pristine and hole doped structures are compared in this section. The subscripts xx and zz are polarization along x and z directions, respectively, giving anisotropic optical behavior of rutile TiO_2.

3.2.1 For pristine system

The $\varepsilon_1(\omega)$ remains positive in the low-energy region, with static dielectric constants of nearly 4.6 (xx) and 5.6 (zz), showing stronger electronic screening along the c-axis [31]. At around 3.3—3.4 eV, clear peaks are observed for both polarization directions due to O(2p) and Ti(3d) transitions. When the photon energy exceeds about 5.3 eV, $\varepsilon_1(\omega)$ becomes negative in both polarization directions.This signifies the beginning of plasmonic behavior and shift towards metallic-like optical response (Figure 4(a)) . In Figure 4(b), $\varepsilon_2(\omega)$ shows photon-induced interband transitions in rutile TiO_2. The absorption edge comes nearly 2.9–3.0 eV, compatible with the mBJ–derived optical band gap. Several absorption peaks are observed throughout the 3–9 eV region, arising from O(2p) and Ti(3d) transitions. The components along xx and zz directions share similar trends, but differences in their peak intensities reveal the intrinsic optical anisotropy of rutile TiO_2.

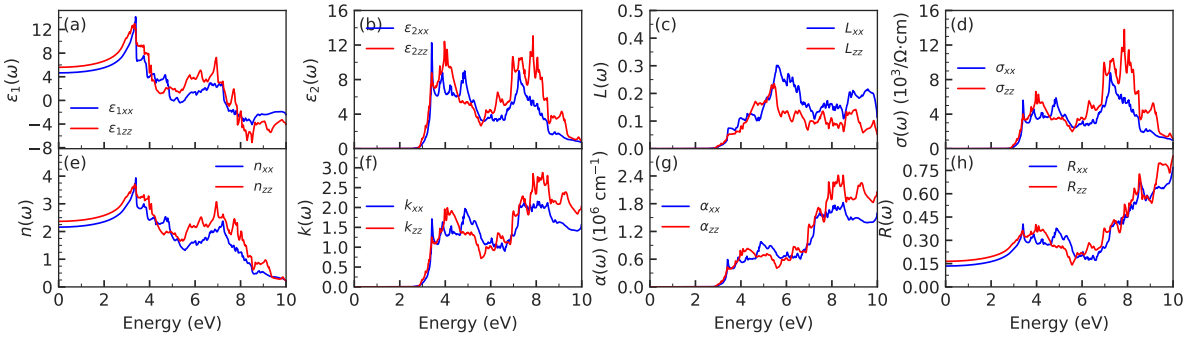

Figure 4: Calculated optical parameters for pristine rutile TiO_2 as functions of photon energy.

Loss function $L(\omega)$ (Figure 4(c)), which describes the rate at which electrons lose energy within the medium. Pronounced peaks appear nearly at 5.47 eV (zz) and 5.48 eV (xx), which correspond to bulk plasmon resonances where $\varepsilon_1(\omega)$ approaches zero and $\varepsilon_2(\omega)$ is minimal. The optical conductivity $\sigma(\omega)$ (Figure 4(d)) follows behavior similar to $\varepsilon_2(\omega)$, since $\sigma(\omega) \propto \omega\varepsilon_2(\omega)$ [32]. Distinct conductivity peaks arise at 3.41 eV and 4.87 eV for x–polarized light, and at 3.41 eV, 3.98 eV and 4.09 eV for z–polarized light, corresponding to strong absorption events driven by photon-induced interband transitions. Some pointed peaks near higher energies may also contain contributions from plasmon-enhanced excitation channels. The refractive index $n(\omega)$ decreases from its static values of nearly 2.16 (xx) and 2.37 (zz) as photon energy increases. Around 3.8–4.0 eV, $n(\omega)$ reaches maxima of 4.0 (xx) and 3.9 (zz) that closely matches the energies where $\varepsilon_1(\omega)$ has strong dispersive peaks (Figure 4(e)). The relatively high $n(\omega)$ in the low-energy region indicates strong interaction of light-matter, supporting suitability of TiO_2 for optoelectronic and photonic applications [33].

Figure 4(f) presents the extinction coefficient $k(\omega)$, which quantifies attenuation of light due to absorption [34]. A sharp increase is observed near 3 eV, and beyond this, $k(\omega)$ continues to increase reaching its maximum value of about 2.7 around 8 eV, indicating stronger electronic transitions at higher photon energies. The absorption coefficient $\alpha(\omega)$ attenuation of optical energy as light traverses the medium. [35]. The absorption edge appears near 3 eV that indicates the origin of interband transitions. After this , $\alpha(\omega)$ increases rapidly (Figure 4(g)). Several absorption bands appear between 3.2–9.5 eV, matching with high-density transition channels. This suggests the efficient UV absorption in rutile TiO_2 . In low-energy region of $R(\omega)$, the reflectance is small (Figure 4(h)). This means the most incident photons are absorbed instead of being reflected. As photon energy increases, reflectivity slowly increases and reaches its maximum nearly at 8.4 eV (xx) and 8.5 eV (zz). Such low reflective behavior across the studied range highlights the potential of TiO_2 for optoelectronic and photonic applications.

3.2.2 For doped system

Figure 5 depictes frequency dependent optical properties of rutile TiO_2 with 10% and 20% Sc doping, calculated using the mBJ potential. Sc doping is treated as effective hole doping, since Sc^{3+} ions substitute Ti^{4+} sites, thereby presenting hole carriers into the system and changing the optical response.

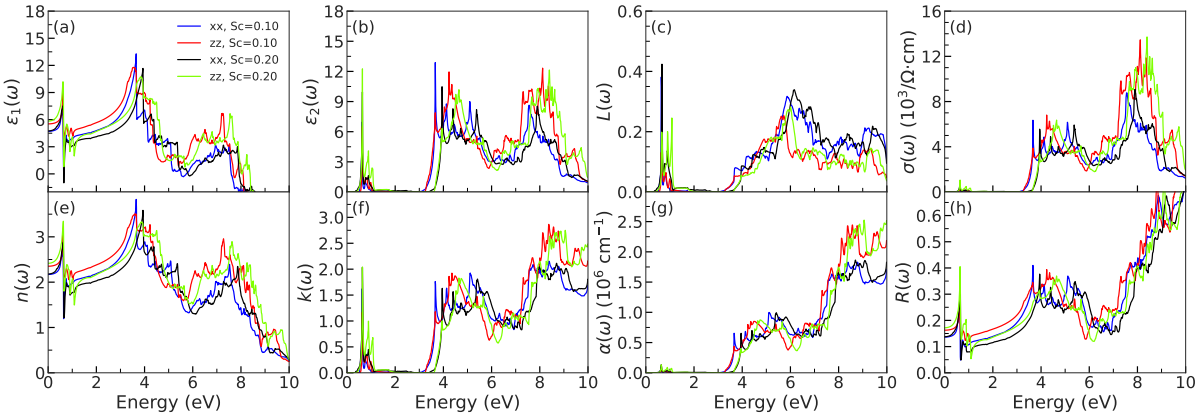

Figure 5: Calculated optical parameters for hole–doped (10% and 20%) rutile TiO_2 as functions of photon energy.

In Figure 5(a) real part $\varepsilon_1(\omega)$, static dielectric constant $\varepsilon_1(0)$ increases with Sc concentration, showing enhanced polarizability induced by hole doping. Compared to undoped TiO_2, which exhibits $\varepsilon_1(0)$ values of nearly 4.6 (xx) and 5.6 (zz), $\varepsilon_1(0)$ rises to nearly 4.8/5.2 for 10% Sc and further to 4.9/5.6 for 20% Sc along the xx/zz directions, respectively. Additionally, the $\varepsilon_1(\omega)$ peaks move toward higher photon energies with increasing Sc content, reflecting doping-induced changes in band structure and a stronger light–matter interaction. In Figure 5(b) imaginary part of $\varepsilon_2(\omega)$ is associated with photon-induced interband transitions. After Sc doping, the absorption edge moves to higher energies from about 3.10 eV for 10% Sc to around 3.61 eV for 20% Sc. This behavior is due to O(2p) and Ti(3d) transitions, indicating that Sc-induced hole doping serves a key function in tuning optical band struc-

ture of TiO_2.

Figure 5(c) shows the loss function $L(\omega)$, which is related to plasmon excitations. Along the xx direction, the plasmon peak remains almost unchanged at around 5.47 eV, indicating that the bulk plasmon behavior is stable under moderate Sc doping. In contrast, along the zz direction, Sc incorporation causes a small shift in the plasmon peak, from about 5.87 eV at 10% Sc to about 6.17 eV at 20% Sc. This suggests that hole doping leads to an anisotropic change in the dielectric response. The optical conductivity $\sigma(\omega)$ (Figure 5(d)) increases with Sc concentration along the zz polarization. For 10% Sc doping, $\sigma(\omega)$ reaches peak values of $\sim 6.3 \times 10^3$ Ω^{-1} cm^{-1} (xx) and $\sim 6.8 \times 10^3$ Ω^{-1} cm^{-1} (zz), while for 20% Sc doping the corresponding values are $\sim 5.6{\times}10^3$ and $\sim 6.4{\times}10^3$ Ω^{-1} cm^{-1}. On comparing with the parent compound, the conductivity peaks are found to be higher after doping, suggesting improved photoconductive response.

As observed in Figure 5(e), refractive index $n(\omega)$ increases to about 2.24 (xx) and 2.84 (zz) for 10% Sc–doping, and to 2.28 (xx) and 2.92 (zz) for 20% Sc–doping. Compared to pristine TiO_2 values of 2.16 (xx) and 2.37 (zz), these increases indicate higher electronic polarizability. The extinction coefficient $k(\omega)$, shown in Figure 5f, indicates clear absorption peaks above 3.5 eV, further supporting the optical enhancement of TiO_2 as Sc concentration increases. In Figure 5(g), the absorption coefficient $\alpha(\omega)$ exhibits a slight shift in the absorption edge with Sc–doping compared to pristine TiO_2 (which appears near 3 eV), indicating enhanced transitions and improved optical activity in the near–UV region.

Finally, Figure 5(h) shows the reflectivity spectra $R(\omega)$. Only small changes in reflectivity are observed with Sc doping. Along the xx direction, the reflectivity decreases slightly as the Sc concentration increases from 10% to 20%. This suggests that hole doping allows some tuning of the surface optical response. Overall, TiO_2 shows low to moderate reflectivity. When combined with the increased absorption and conductivity, these results indicate that Sc substitution is effective in modifying the optical properties of TiO_2, making it suitable for optoelectronic and photonic applications.

4 Conclusion

We implemented density functional theory to study electronic and optical properties of pristine and hole-doping in rutile TiO_2. The pristine material is found to be a direct band gap semiconductor (2.35 eV), suitable for optical applications. With increasing hole concentration on the Ti site, the Fermi level shifts toward the valence region. The material shows optical activity in the visible and lower UV range. In hole-doped TiO_2, the dielectric constants and refractive indices increase, and the absorption edge shifts slightly toward higher energies, showing clear anisotropy. With increasing Sc doping concentration from 10% to 20%, suggest that hole-doped rutile TiO_2 is promising material for optoelectronic devices.

Acknowledgements

The authors acknowledge Prof. Dr. Hari Prasad Lamichhane, Dipak Bhattarai, and Deergh Bahadur Shahi for taking part in a group discussion regarding this research.

Author contribution

K.K. performed DFT calculations for electronic properties, conducted data analysis, and contributed to manuscript writing. N.S. assisted with data analysis and manuscript writing. D.P.K. carried out DFT calculations for optical properties, visualized results. M.K. contributed to manuscript revision. M.P.G. provided supervision and manuscript revision. T.R.L. offered critical feedback, technical support, and contributed to manuscript revision.

Declaration

The authors have no competing interest.

Data Availability

The data supporting this study's findings are provided within the article.

References

[1] A. Fujishima and K. Honda. Electrochemical photolysis of water at a semiconductor electrode. *Nature*, 238(5358):37–38, 1972.

[2] X. Chen and S.S. Mao. Titanium dioxide nanomaterials: synthesis, properties, modifications, and applications. *Chemical Reviews*, 107(7):2891–2959, 2007.

[3] U. Diebold. The surface science of titanium dioxide. *Surface Science Reports*, 48(5-8):53–229, 2003.

[4] M. Song, Z. Lu, and D. Li. Phase transformations among TiO_2 polymorphs. *Nanoscale*,

12(45):23183–23190, 2020.

[5] J. Zhang, P. Zhou, J. Liu, and J. Yu. New understanding of the difference of photocatalytic activity among anatase, rutile, and brookite TiO_2. *Physical Chemistry Chemical Physics*, 16(38):20382–20386, 2014.

[6] J. Moma and J. Baloyi. Modified titanium dioxide for photocatalytic applications. *Photocatalysts-Applications and Attributes*, 18(10):5772, 2019.

[7] H. Khan and M.U.H. Shah. Modification strategies of TiO_2-based photocatalysts for enhanced visible light activity and energy storage ability: A review. *Journal of Environmental Chemical Engineering*, 11(6):111532, 2023.

[8] K. Yang, Y. Dai, and B. Huang. First-principles calculations for geometrical structures and electronic properties of Si-doped TiO_2. *Chemical Physics Letters*, 456(1-3):71–75, 2008.

[9] S. Muthukrishnan, R. Vidya, and A.O. Sjaastad. Band gap engineering of anatase TiO_2 by ambipolar doping: A first principles study. *Materials Chemistry and Physics*, 299:127467, 2023.

[10] L.A. May Ix, A. Estrella Gonzalez, S. Cipagauta-Diaz, and R. Gomez. Effective electron–hole separation over n-doped TiO_2 materials for improved photocatalytic reduction of 4-nitrophenol using visible light. *Journal of Chemical Technology and Biotechnology*, 95(10):2694–2706, 2020.

[11] B.G. Park. Photocatalytic activity of TiO_2-doped Fe, Ag, and Ni with N under visible light irradiation. *Gels*, 8(1):14, 2021.

[12] V. Stengl, S. Bakardjieva, and N. Murafa. Preparation and photocatalytic activity of rare earth doped TiO_2 nanoparticles. *Materials Chemistry and Physics*, 114(1):217–226, 2009.

[13] A. Khlyustova, N. Sirotkin, T. Kusova, A. Kraev, V. Titov, and A. Agafonov. Doped TiO_2: the effect of doping elements on photocatalytic activity. *Materials Advances*, 1(5):1193–1201, 2020.

[14] P. Basera, S. Saini, E. Arora, A. Singh, M. Kumar, and S. Bhattacharya. Stability of nonmetal dopants to tune the photo-absorption of TiO_2 at realistic temperatures and oxygen partial pressures: A hybrid DFT study. *Scientific Reports*, 9(1):11427, 2019.

[15] S. Zahan and M. A. Rashid. Electronic, magnetic, and optical properties of Nb-doped rutile TiO_2: Insights from DFT. *Insights from DFT*, 2022.

[16] W. Zhou and N. Umezawa. Viable approach toward efficient p-type conductivity in Al-doped anatase TiO_2 via strain engineering. *RSC Advances*, 7(33):20542–20547, 2017.

[17] J.K. Burdett, T. Hughbanks, G.J. Miller, James W. Richardson J., and J.V. Smith. Structural-electronic relationships in inorganic solids: powder neutron diffraction studies of the rutile and anatase polymorphs of titanium dioxide at 15 and 295 K. *Journal of the American Chemical Society*, 109(12):3639–3646, 1987.

[18] K. Koepernik and H. Eschrig. Full-potential nonorthogonal local-orbital minimum-basis band-structure scheme. *Physical Review B*, 59(3):1743, 1999.

[19] J.P. Perdew, K. Burke, and M. Ernzerhof. Generalized gradient approximation made simple. *Physical Review Letters*, 77(18):3865, 1996.

[20] F. Tran and P. Blaha. Accurate band gaps of semiconductors and insulators format with a semilocal exchange-correlation potential. *Physical Review Letters*, 102(22):226401, 2009.

[21] D. Koller, F. Tran, and P. Blaha. Merits and limits of the modified Becke-Johnson exchange potential. *Physical Review B—Condensed Matter and Materials Physics*, 83(19):195134, 2011.

[22] L. Chiodo, J.M. Garcia-Lastra, A. Iacomino, S. Ossicini, J. Zhao, H. Petek, and A. Rubio. Self-energy and excitonic effects in the electronic and optical properties of TiO_2 crystalline phases. *Physical Review B*, 82(4):045207, 2010.

[23] A. Thilagam, D.J. Simpson, and A.R. Gerson. A first-principles study of the dielectric properties of TiO_2 polymorphs. *Journal of Physics: Condensed Matter*, 23(2):025901, 2010.

[24] S.P. Kowalczyk, F.R. McFeely, L. Ley, V.T. Gritsyna, and D.A. Shirley. The electronic structure of $SrTiO_3$ and some simple related oxides (MgO, Al_2O_3, SrO, TiO_2). *Solid State Communications*, 23(3):161–169, 1977.

[25] R. Asahi, Y. Taga, W. Mannstadt, and A.J. Freeman. Electronic and optical properties of anatase TiO_2. *Physical Review B*, 61(11):7459, 2000.

[26] D.P. Rai, A. Shankar, M.P. Ghimire, R.K. Thapa, et al. The electronic, magnetic,

and optical properties of double perovskite A_2FeReO_6 (A = Sr, Ba) from first principles approach. *Computational Materials Science*, 101:313–320, 2015.

[27] G.B. Acharya, S.H. Kim, and M.P. Ghimire. Electronic and optical properties of ternary kagome $Rb_2Ni_3S_4$: a density functional study. *Modelling and Simulation in Materials Science and Engineering*, 32(6):065012, 2024.

[28] D.P. Kalauni, K.N. Jaiswal, S. Lawaju, K.B. Rai, R.J. Yadav, A.D. Mishra, and M.P. Ghimire. Electronic and optical properties of halogen-substituted $LaBi_2Cl_{1-y}X_yO_4$: a promising candidate for energy-efficient devices. *RSC Advances*, 15(43):35930–35940, 2025.

[29] H. He, R. Orlando, M.A. Blanco, R. Pandey, E. Amzallag, I. Baraille, and M. Rerat. First-principles study of the structural, electronic, and optical properties of Ga_2O_3 in its monoclinic and hexagonal phases. *Physical Review B—Condensed Matter and Materials Physics*, 74(19):195123, 2006.

[30] S. R. Bhandari, D. K. Yadav, B. P. Belbase, M. Zeeshan, B. Sadhukhan, D. P. Rai, R. K. Thapa, G. C. Kaphle, and M. P. Ghimire. Electronic, magnetic, optical and thermoelectric properties of $Ca_2Cr_{1-x}Ni_xOsO_6$ double perovskites. *RSC Advances*, 10(27):16179–16186, 2020.

[31] J.S. Toll. Causality and the dispersion relation: logical foundations. *Physical Review*, 104(6):1760, 1956.

[32] D.M. Hoat, J.F.R. Silva, and A.M. Blas. Systematic study of structural, electronic, optical and thermodynamic properties of SrFCuTe compound. *Journal of Solid State Chemistry*, 270:85–91, 2019.

[33] P. Joshi, G.B. Acharya, I.B. Khadka, B. Srinivasan, S. Kim, and M.P. Ghimire. Enhanced optoelectronic and thermoelectric properties in kagome $Rb_2Pt_3S_4$: a probable energy-efficient material. *ACS Applied Energy Materials*, 8(5):3217–3228, 2025.

[34] T.Y. Ahmed, S.B. Aziz, and E.M.A. Dannoun. New photocatalytic materials based on alumina with reduced band gap: A DFT approach to study the band structure and optical properties. *Heliyon*, 10(5), 2024.

[35] M. Zanib, M.W. Iqbal, M. Manzoor, M. Asghar, R. Sharma, N.N. Ahmad, S.M. Wabaidur, M.A. Habila, S.A.M. Abdelmohsen, A.M.M. Abdelbacki, et al. A DFT investigation of mechanical, optical, and thermoelectric properties of double perovskites K_2AgAsX_6 (X = Cl, Br) halides. *Materials Science and Engineering: B*, 295:116604, 2023.